Available online at www.sciencedirect.com
SCIENCE DIRECT®
Journal of Power Sources 142 (2005) 169–176
JOURNAL OF POWER SOURCES
www.elsevier.com/locate/jpowsour

Alternative supports for the preparation of catalysts for low-temperature fuel cells: the use of carbon nanotubes

M. Carmo[a], V.A. Paganin[a], J.M. Rosolen[b], E.R. Gonzalez[a,*]

[a] *Instituto de Química de São Carlos/USP, CP 780, CEP 13560-970 São Carlos, SP, Brazil*
[b] *Faculdade de Filosofia Ciências e Letras de Ribeirão Preto/USP, Depto de Química, Av. Bandeirantes, 3900, CEP 14040-901 Ribeirão Preto, SP, Brazil*

Received 21 September 2004; accepted 20 October 2004
Available online 29 December 2004

Abstract

Noble metal catalysts in the form of nanoparticles supported on high surface area carbon exhibit characteristics which depend strongly on the nature of the support. This work presents results with noble metal catalysts supported on carbon nanotubes (MWNT and SWNT) and also on a high surface area carbon powder Vulcan XC-72, for proton exchange membrane fuel cells (PEMFC) fed with hydrogen contaminated with CO and also for the direct methanol fuel cell (DMFC). A high performance was achieved with PtRu supported on nanotubes for H_2 + 100 ppm CO, although it was similar to that presented by PtRu on Vulcan XC-72 with an overpotential of 100 mV at 1 A cm^{-2}. Results for the DMFC showed power densities exceeding 100 mW cm^{-2} at 90 °C and 0.3 MPa and the activity of the anodes followed the sequence: PtRu/MWNT > PtRu/Vulcan XC-72 > PtRu/SWNT. The electrocatalysts were all prepared with the same method, namely impregnation of the carbons with the precursors in ethanol and reduction under a hydrogen atmosphere. The role of Ni, Fe and other contaminants contained in the as-received carbon nanotubes is discussed.

Keywords: Carbon nanotubes; DMFC; PEMFC; Electrocatalysis; CO oxidation

1. Introduction

Two of the most advanced low-temperature fuel cells are the proton exchange membrane fuel cell (PEMFC) and the direct methanol fuel cell (DMFC). Both are low-temperature fuel cells that working with plain Nafion® membranes operate at temperatures that rarely exceed 80 and 130 °C, respectively. At these temperatures, it is essential the use of CO-tolerant electrocatalysts [1,2] to deal with the CO contained in the hydrogen obtained by steam reforming of other fossil or renewable fuels or formed as intermediate in the complex oxidation process of methanol. Pt-based electrocatalysts display the necessary stability in the acidic environments of the PEMFC and DMFC and, although much progress is still needed, they show significant activity. However, CO can adsorb very strongly on the Pt surface in the fuel cell anode [3], blocking the active sites and causing a large decrease in the electrode performance. In order to reduce this poisoning problem, the utilisation of a second metal able to form oxygenated species at lower potentials than pure Pt has been proposed and described [4,5]. Following a bifunctional mechanism, the metal–OH species act as a source of atomic oxygen, required for the oxidation of CO to CO_2, liberating active sites on the surface of the catalyst material near a platinum atom, where the adsorption and oxidation of the gaseous hydrogen takes place [6]. Also, spectroscopic studies on polycrystalline Pt have shown that methanol is electrosorbed in a complex process analogous to a dehydrogenation. Sequen-

* Corresponding author. Tel.: +55 16 3373 9899/9951; fax: +55 16 3373 9952.
E-mail addresses: mcarmo@iqsc.usp.br (M. Carmo), vpaganin@iqsc.usp.br (V.A. Paganin), rosolen@ffclrp.usp.br (J.M. Rosolen), ernesto@iqsc.usp.br (E.R. Gonzalez).

0378-7753/$ – see front matter © 2004 Elsevier B.V. All rights reserved.
doi:10.1016/j.jpowsour.2004.10.023

tial stripping of protons and electrons is believed to take place leading to the formation of carbon-containing intermediates, such as linearly bonded $-CO_{ads}$ and $-CHO_{ads}$ [7,8].

Among the several possibilities of using binary alloys, the PtRu alloy has shown the most promising performance for the hydrogen oxidation reaction in the presence of CO [9,10] and also for the oxidation of methanol [11]. While a typical DMFC is less efficient than a PEMFC, work to improve its performance with new electrocatalyst materials has proved successful. In almost all cases, carbon blacks have been used as support of the metal nanoparticles, particularly Vulcan XC-72 (Cabot) which has a surface area of 240 $m^2\ g^{-1}$. However, in recent years there has been a progress in the understanding of electronic effects in the metal catalyst, in which not only alloying but also the catalyst–support interaction play a fundamental role. Because of this, it is of interest to explore the behaviour of Pt-based catalysts prepared on supports different from those most frequently used.

Carbon nanotubes are prominent materials that exhibit special properties which make them suitable for application in several technological areas [12]. In the fuel cell area, they could be of interest as catalyst supports [13] and also as hydrogen storage materials [14]. This work presents results with electrodes prepared with Pt and PtRu as electrocatalysts supported on nanotubes and, for comparison, on the most usual support, Vulcan XC-72. The catalysts were prepared by a modification of a method described in the literature [15], and tested in electrochemical half-cells and single-fuel cells.

2. Experimental

Single-wall carbon nanotubes (SWNT) were prepared by the arc-discharge method in the laboratories of the University of São Paulo at Ribeirao Preto [16]. The catalyst mixture was prepared using as metallic elements Fe:Ni:Co in the atomic ratio 1:1:1. A partial atmosphere of high-purity helium at 0.053 MPa was used and also a high current of 120 A. The material collected was mainly the soot from the collar because it was found to be richer in SWNTs than that from the cathode deposit or the interior wall [17]. The multi-wall carbon nanotubes (MWNT) were commercially available (SUN Nanotech Co. Ltd.). Vulcan XC-72 (E-TEK) was pre-treated in an argon atmosphere at 850 °C for 5 h [18] before use.

The Pt and PtRu carbon-supported catalysts (20 wt.% metal/C) were prepared from H_2PtCl_6 (Johnson Matthey) and $RuCl_3$ (Aldrich) by the following procedure: the carbon support was impregnated with an ethanol solution of the precursors under sonication for 3 h and then the ethanol was evaporated at 80 °C. The dry impregnated carbon support was placed in alumina boats, submitted to an additional drying step under an argon atmosphere at 100 °C for 1 h and then the decomposition/reduction of the metal precursors was carried out at 550 °C under a pure hydrogen flow for 3 h.

The composition of the prepared catalysts was determined by energy-dispersive X-ray analysis (EDX) in a scanning electron microscope LEO, 440 SEM-EDX system (Leica-Zeiss, DSM-960) provided with a microanalyser (Link Analytical QX 2000) and a detector of SiLi using a 20-keV electron beam.

The catalysts were also examined by X-ray diffraction techniques (XRD) using a URD-6 Carl Zeiss-Jena diffractometer. The X-ray diffractograms were obtained with a scan rate of 3° min^{-1} and an incident wavelength of 1.5406 Å (Cu Kα). The XRD data were used to estimate the Pt lattice parameter and, using Scherrer's equation [19], the average crystallite size.

Two-layer (diffusion layer and catalyst layer) gas diffusion anodes were prepared with the supported materials using the methodology employed previously in these laboratories [1,2,20,21]. In all cases, the gas diffusion cathodes were prepared with Pt/C commercial catalyst (20 wt.% Pt/Vulcan XC-72, E-TEK). Other materials used were Nafion® solution (DuPont, ∼5.5 wt.%), polytetrafluorethylene suspension (Teflon® TE 306 A, DuPont), carbon powder (Vulcan XC-72, E-TEK), and carbon cloth (PWB-3, Stackpole®). The carbon cloth was previously covered on both sides with a mixture of PTFE suspension and Vulcan XC-72 carbon and sintered at 330 °C to form a diffusion layer. Then the catalytic layer composed of the Pt/C or PtRu/C catalysts and Nafion® solution was applied on one side. The electrode was then heated for 1 h at 80 °C [20].

The membrane and electrode assemblies (MEAs) were prepared by hot-pressing two electrodes on both sides of a pre-treated Nafion® 115 membrane (H^+, DuPont) [20] at 125 °C and 5 MPa for 2 min. The electrodes had a geometric area of 4.6 cm^2 and the noble metal content was 0.4 mg cm^{-2}. The MEA was placed between high-density carbon plates in which serpentine-type channels were machined for the circulation of O_2, H_2, H_2 + 100 ppm CO or CH_3OH solutions.

Solutions were prepared with pure water (18.2 MΩ cm, Millipore Milli Q®) and methanol (J. T. Backer, p.a.). The gases were: argon (99.998%), nitrogen (99.996%), carbon monoxide (99.5%) and hydrogen or oxygen (pre-purified), all from White Martins.

The half-cell data were obtained using a Solartron 1285 potentiostat and the software Corrware, and those with a single-fuel cell were obtained using an Electronic Load HP 6050A.

The H_2/O_2 PEMFC polarisation experiments were carried out galvanostatically with the cell at 85 °C, using O_2 saturated with water at 90 °C and 0.17 MPa in the cathode, and either pure hydrogen or a mixture of H_2/100 ppm CO saturated with water at 100 °C and 0.2 MPa in the anode. Before the data acquisition, the system was maintained at a cell potential of 0.7 V with pure H_2 for 2 h and at 0.8 V with H_2/100 ppm CO for a further 2 h.

The DMFC polarisation experiments were also carried out galvanostatically with the cell at 70 °C using pure O_2 saturated with water at 70 °C and atmospheric pressure or with the cell at 90 °C and O_2 saturated with water at 90 °C and 0.3 MPa. In all experiments, the flows of O_2 gas and of the

2 mol L^{-1} methanol solution were 80 and 2 ml min^{-1}, respectively. Before data acquisition, the system was maintained under a current density of 0.2 A cm^{-2} for at least 6 h at 90 °C and O_2 pressurised at 0.3 MPa.

The CO stripping experiments were carried out as follows: after the electrosorption of CO under potentiostatic control at 50 mV (versus RHE) for a period of 30 min the cell was flushed with N_2 for a further 30 min to remove any unreacted CO and finally the anode potential was scanned at 10 mV s^{-1} up to 0.9 V (versus RHE).

The methanol stripping experiments were carried out in a similar way: methanol was adsorbed from a 2 mol L^{-1} solution at 75 mV (versus RHE) under potentiostatic control for a period of 40 min. The cell was then flushed with water for a further 20 min and the stripping scan recorded at 10 mV s^{-1} up to 0.9 V (versus RHE). In these stripping experiments, the electrolyte was only the wet Nafion® polymer.

3. Results and discussion

Table 1 presents the results from the EDX analyses, which show small discrepancies when compared with the nominal compositions expected from the relative amounts of precursors used in the preparation of the noble metal catalysts. On the other hand, the EDX analyses show that carbon nanotubes contain appreciable amounts of Ni, Fe and Co used in their production by the arc method [17]. The presence of these metals may certainly affect the characteristics of the catalysts and will be taken into account in some of the discussions below.

Fig. 1 shows the X-ray diffraction patterns for the prepared catalysts. In all cases, the peaks observed indicate the presence of the face-centred cubic structure typical of platinum metal, represented by the crystalline planes (1 1 1), (2 0 0), (2 2 0), and (3 1 1) (JCPDS, card 4-802) and also some reflections characteristics of carbon (identified as C [22]). Peaks characteristic of the reflections of Ni (JCPDS, card 4-850), Fe (JCPDS, card 6-696) and Co (JCPDS, card 5-727) contained in the carbon nanotubes, and also those associated to metallic Ru (JCPDS, card 6-663) were not observed. Indeed, if the reflection intensities of the other metals are low compared with those of platinum and/or the metals are present

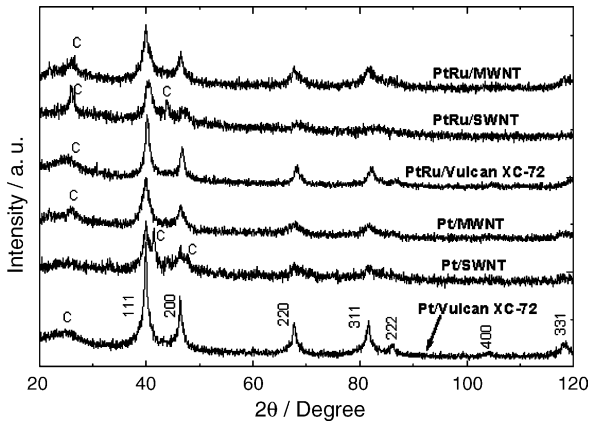

Fig. 1. X-ray diffractograms of the prepared catalysts on the different carbon supports. λ = 1.54056 Å (Cu Kα).

as amorphous compounds they will not be detected in the diffractograms. A less likely possibility is that in the preparation procedure the nanotube contaminants were covered by platinum to the point of not being detected. The presence of ruthenium incorporated as a substitution in the platinum structure is noted through the shift of the Bragg angles with respect to the values for pure platinum.

The crystallite size of the catalysts was estimated from the XRD data using Scherrer's equation. For this purpose, the (2 2 0) reflection was used. Although it is not the strongest, it is outside the region of the broad band produced by the carbon support. For Pt on both types of nanotubes, the particle size was almost the same (3.62 nm) while for Pt supported on Vulcan XC-72 it was significantly higher (6.83 nm). This is an interesting result and suggests that the nanotube morphological structure favours the dispersion of the electrocatalyst on the support by preventing the coalescence of the growing nuclei. The large differences in particle size cannot be explained by the presence of the other metals in the nanotubes. Similar differences were observed for PtRu. The crystallite size of PtRu supported on the nanotubes was between 4.06 to 4.62 nm, while that of the PtRu on Vulcan XC-72 was much higher (6.39 nm). It has been suggested that Ru promotes the dispersion of the electrocatalyst; the unalloyed amorphous material that may reside on or near the surface of the PtRu alloy particles may help prevent sintering during the deposition

Table 1
EDX composition of the supports and of the catalysts on the supports

Material	Metal/atom (%)					XRD crystallite size (nm)	XRD lattice parameter (nm)
	Pt	Ru	Fe	Ni	Co		
MWNT	–	–	59	40	1	–	–
SWNT	–	–	30	36	34	–	–
20 wt.% Pt/MWNT	80	–	12	6	2	3.62	0.39171
20 wt.% Pt/SWNT	50	–	17	17	16	3.62	0.38842
20 wt.% Pt/Vulcan XC-72	100	–	–	–	–	6.83	0.39099
20 wt.% PtRu/MWNT	50	40	5	5	0	4.62	0.38997
20 wt.% PtRu/SWNT	28	20	20	18	14	4.06	0.38704
20 wt.% PtRu/Vulcan XC-72	55	45	–	–	–	6.39	0.38834

The crystallite sizes and the lattice parameters for the Pt/C and PtRu/C catalysts, from XRD, are also included.

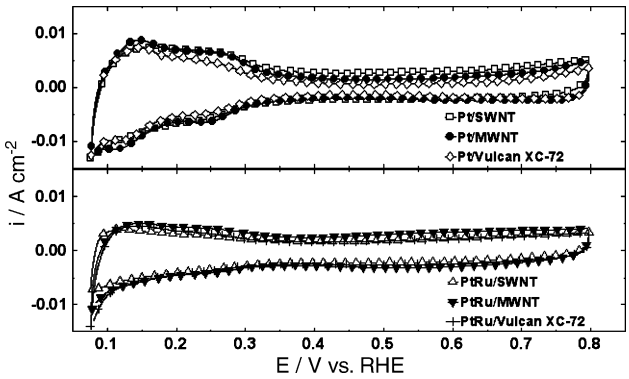

Fig. 2. Cyclic voltammograms in a single cell for anodes (fed with N_2) with several Pt and PtRu carbon-supported catalysts (20 wt.% metal/C, 0.4 mg noble metal cm^{-2}). Cathodes (fed with H_2) with 20 wt.% Pt/C (E-TEK, 0.4 mg Pt cm^{-2}). Nafion® 115 membrane. $T = 27 \pm 2\,^{\circ}C$. Current density with respect to geometric area, $v = 20\,mV\,s^{-1}$.

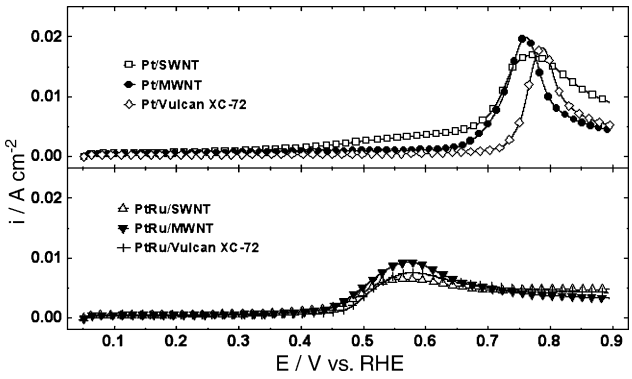

Fig. 3. Stripping scans for electrosorbed CO for the Pt/C and PtRu/C anodes of Fig. 2. Electrosorption at 50 mV (vs. RHE) with CO for 30 min and flushing with N_2 for 30 min. Potential scanned to 0.9 V (vs. RHE) at $10\,mV\,s^{-1}$.

or during the thermal reduction processes [11]. This explains the smaller particle size for PtRu/Vulcan XC-72 as compared with the Pt/Vulcan XC-72 catalyst. The values of the XRD lattice parameter were in all cases smaller than the value for pure Pt (0.39231 nm, JCPDS card 4-802). This is due to the interactions with the supports and/or the insertion of other metals into the fee lattice of platinum, like the contaminants of the nanotubes and also ruthenium in the PtRu/C catalysts [21].

Fig. 2 shows the cyclic voltammograms for Pt and PtRu anodes prepared on the different supports. The half-cell behaviour of the anodes was studied by supplying hydrogen to the cathode, which then functioned as a reversible hydrogen electrode (RHE) and also as a counterelectrode, with the Nafion® acting as the electrolyte. The cyclic voltammograms present characteristics for each type of catalyst, which depend on the metal [18]. The hydrogen upd region (0.075–0.35 V versus RHE) in Pt catalysts is well defined, while for PtRu catalysts is less defined because the hydrogen adsorption/desorption peaks are not developed on Ru. The double-layer region of the PtRu/C catalysts is larger than for Pt/C, both because of the formation of more oxygenated species and also of a larger surface area due to a smaller particle size.

Fig. 3 shows the CO_{ads} stripping scans recorded for each electrocatalyst. It can be observed that the onset of the current for CO oxidation appears at lower potential values for Pt/nanotubes as compared to Pt/Vulcan XC-72. Originally, the carbon nanotubes contain Ni, Fe and other contaminants [16,17], detected in the EDX analyses, which may form oxygenated species that contribute to the CO oxidation [23]. In a recent paper [24], the adsorption and subsequent oxidation of CO on MWNT was attributed to an enhanced activity of the nanotubes. However, the authors do not seem to take into account the presence of contaminant metals. It is interesting to note the presence of a shoulder on the Pt/SWNT CO stripping peak, which suggests that the electrocatalyst contains either two types of reaction sites and/or crystallites with different activities. On the other hand, in the PtRu material deposited onto different supports the main contribution to the shift of the peak to lower potential values is the presence of Ru. This occurs because Ru is more easily electrooxidised than pure Pt, and forms $Ru–OH_{ads}$ species at lower potentials, which help to oxidise the adsorbed CO through the bifunctional mechanism. Also, it must be taken into account that in the alloy a weakening of the Pt–CO bond takes place, resulting in a lower CO coverage and an increased mobility similar to what happens with other CO-tolerant Pt alloys, via the modification of the Pt electronic structure by alloying [23].

The results of the integration of the peaks for CO stripping presented in Fig. 3 are summarised in Table 2, in the form of the CO electrochemical active area for each electrocatalyst. These values correspond to the total metal surface area in contact with the proton-conducting polymer in the electrodes, i.e. total active sites available for the oxidation of CO. For the 20 wt.% Pt/Vulcan XC-72 catalyst, the values agree well with the values determined by the charge due to the adsorption of hydrogen (see Table 2), but for Pt/nanotube electrocatalysts the CO chemisorption metal area is higher than that determined by H_2 adsorption probably due to the contribution of the metal contaminants originally present in the nanotubes. These metals, as well as Ru, are active for the adsorption of CO but do not adsorb hydrogen.

Although the values in Table 2 are normalised for the Pt and Ru content in the PtRu electrocatalysts, it is not clear how the Ru species interact with CO in the electrochemical experiments. For example, metallic Ru or Ru oxides may not be covered with a complete monolayer of CO during the electrochemical measurements [11]. Also, the adsorption of CO is probably dependent on time, temperature and the particle size of the electrocatalyst [11]. However, for lack of more reliable methods, the CO stripping charges constitute the preferred method to determine electrochemically active areas for the type of alloy catalysts studied here.

Table 2 also shows the theoretical (calculated from the XRD particle sizes assuming that the particles are spherical) metal surface areas for the different catalysts. A comparison

Table 2
Active areas of the Pt/C and PtRu/C prepared electrocatalysts determined by different methods

Catalyst	XRD-calculated metal area ($m^2\ g^{-1}$ PtRu)	H_2 chemisorption metal area ($m^2\ g^{-1}$ Pt)	CO chemisorption metal area ($m^2\ g^{-1}$ PtRu)
20 wt.% Pt/SWNT	77	51	69
20 wt.% Pt/MWNT	77	71	80
20 wt.% Pt/Vulcan XC-72	41	64	62
20 wt.% PtRu/SWNT	80	–	49
20 wt.% PtRu/MWNT	71	–	82
20 wt.% PtRu/Vulcan XC-72	51	–	66

between the values of the theoretical and electrochemical (from CO-stripping voltammetry) metal surface areas does not show a definite trend but it is interesting to note that in certain cases the CO active area is larger, which seems a contradiction. This is difficult to rationalise and suggests that for the catalysts supported onto MWNT and Vulcan XC-72 carbons the electrochemical cycling could be promoting a break of some clusters with an increase of active area [25]. Differently, for catalysts supported onto SWNT the CO-stripping metal surface area is always lower than the XRD-calculated area. Another possibility is to consider that CO can be adsorbed and oxidised on the nanotubes as suggested by He et al. [24], but this cannot be stated unambiguously without separating the effect of the contaminant metals.

Fig. 4 shows steady-state polarisation curves for Pt/C anodes (0.4 mg Pt cm^{-2}) fed with pure hydrogen and hydrogen containing 100 ppm CO. As expected, the performance of the Pt/Vulcan XC-72 catalyst drops considerably when the CO-containing H_2 is introduced in the anode. On the other hand, the results for Pt/nanotube catalysts show that the performance with H_2 + 100 ppm CO drops but it is higher than that for Pt/Vulcan XC-72. At this stage it is difficult to say to what extent this is an effect promoted by the characteristics of the catalysts supported on the nanotubes and to what extent there is a beneficial effect of the contaminant metals present in the nanotubes [23].

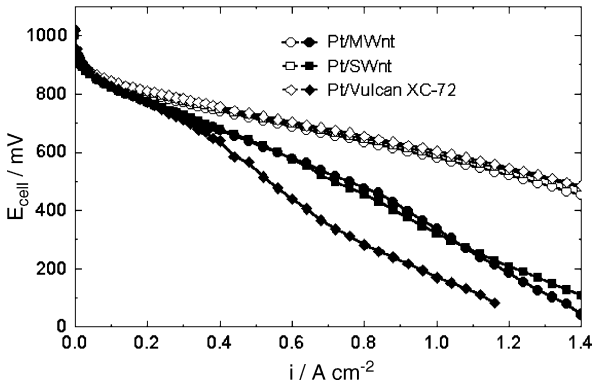

Fig. 4. Potential vs. current density for Pt/C anodes with 0.4 mg Pt cm^{-2}. Cathodes with Pt/C E-TEK, 0.4 mg Pt cm^{-2}. Nafion® 115 membrane. Anodes fed with H_2 (open symbols) or H_2 + 100 ppm of CO (solid symbols) humidified at 100 °C and 0.2 MPa. Cathodes fed with O_2 humidified at 90 °C and 0.17 MPa. Current density with respect to geometric area.

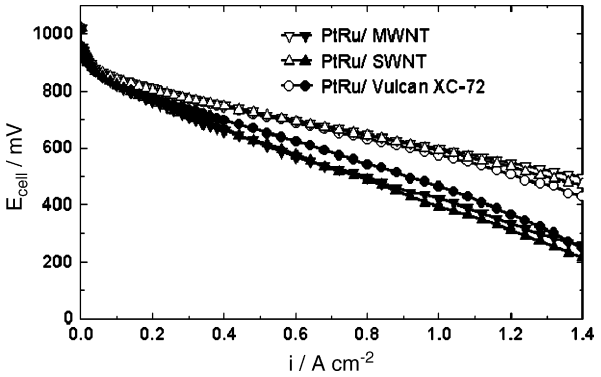

Fig. 5. Potential vs. current density for PtRu/C anodes with 0.4 mg noble metal cm^{-2} on different supports. Other conditions as in Fig. 4.

For the PtRu/C catalysts, the performance with pure H_2 and with H_2 + 100 ppm CO is presented in Fig. 5. It appears that for these alloy catalysts, the contaminants of the nanotube supports do not contribute much to the end results, because the performance of the PtRu/nanotube catalysts is similar to that of the PtRu/Vulcan XC-72. This is consistent with the fact that the CO stripping peaks (Fig. 3) for PtRu/nanotube catalysts are similar to those for PtRu deposited on Vulcan XC-72 carbon. The small difference in favour of the PtRu/Vulcan XC-72 shown in Fig. 5 may not be significant.

Fig. 6 shows potential–current curves for Pt/C and PtRu/C anodes with 0.4 mg noble metal cm^{-2}, in which the potential axis is the difference between the potential of anodes fed with pure H_2 and the same anodes fed with H_2 + 100 ppm CO,

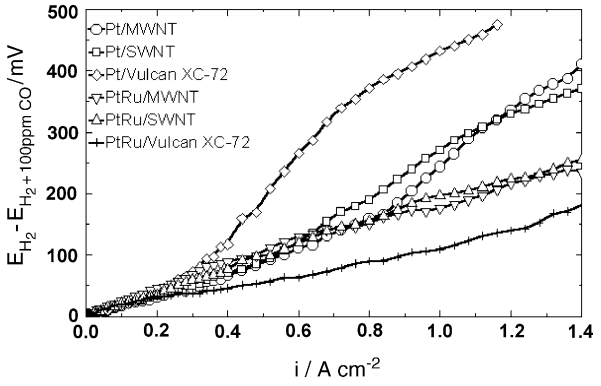

Fig. 6. Overpotential (see text) vs. current density curves for Pt/C and PtRu/C anodes. Same conditions as in Fig. 4.

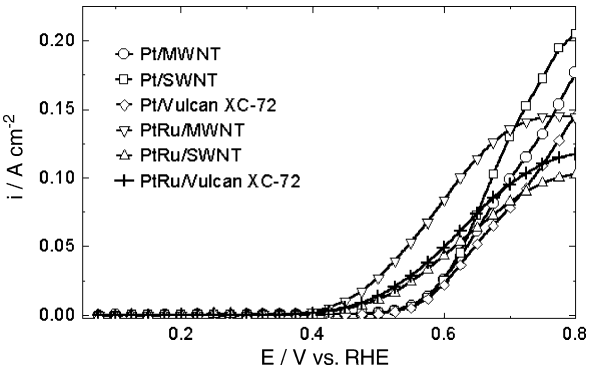

Fig. 7. Current-interrupt corrected polarisation curves for Pt/C and PtRu/C catalysts at room temperature ($27 \pm 2\,^{\circ}C$). Anode supplied with $2\,mol\,L^{-1}$ methanol fuel and the counterelectrode with pure hydrogen. Current density with respect to geometric area.

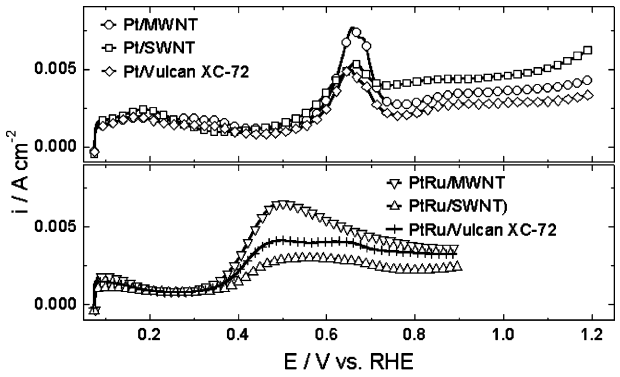

Fig. 8. Stripping peaks of electrosorbed methanol for the Pt/C and PtRu/C anodes of Fig. 7. Electrosorption at 75 mV (vs. RHE) in a $2\,mol\,L^{-1}$ methanol solution (40 min), flushing with water (20 min). Anode potential scanned up to 0.9 V (vs. RHE) at $10\,mV\,s^{-1}$. Room temperature ($27 \pm 2\,^{\circ}C$). Current density with respect to geometric area.

at the same current density. Up to $0.7\,A\,cm^{-2}$ Fig. 6 shows that Pt/MWNT, Pt/SWNT, PtRu/MWNT and PtRu/SWNT present similar, low overpotentials as defined for these experiments. A still lower overpotential is observed with the PtRu/Vulcan XC-72 anode, while the highest is presented by Pt/Vulcan XC-72. The results with PtRu/Vulcan XC-72 in Fig. 6 are similar to those found by Camara et al. [2].

The same membrane and electrode assemblies (MEAs) were used to carry out experiments for the oxidation of methanol in a DMFC set up. In half-cell experiments, the anode of the MEA was supplied with a $2\,mol\,L^{-1}$ methanol solution and the counterelectrode with pure hydrogen, which in this way operated also as a reversible hydrogen electrode. The fuel cell was then driven by a potentiostat and the resistance of the MEA was determined using current-interrupt techniques. Fig. 7 shows the results of these half-cell experiments at $27 \pm 2\,^{\circ}C$. It can be observed that methanol oxidation starts at lower potential values for all the PtRu/C catalysts than for Pt/C anodes. PtRu/MWNT presents the higher activity, while that of PtRu/Vulcan XC-72 and PtRu/SWNT are similar. Among the Pt/C anodes, a different trend can be observed and the sequence of activities is: Pt/SWNT > Pt/MWNT > Pt/Vulcan XC-72. However, it must be pointed out that potentials at which the Pt/C materials present activity are too high and consequently not useful for a DMFC.

The intrinsic activity of the electrocatalysts appears to be linked to a number of factors including electrocatalyst utilisation (the extent of the electrocatalyst/ionomer interface), the thickness of the electrocatalyst layer and its porosity [11]. Fig. 8 shows the stripping peaks of an intermediate species (unknown but it is believed to be a $-CO_{ads}$-like [11]) after adsorption at 0.075 V (versus RHE) in a $2\,mol\,L^{-1}$ methanol solution and then scanning the anode potential up to 0.9 V (versus RHE) at a rate of $10\,mV\,s^{-1}$. In the Ru-containing electrocatalysts, it can be observed that the onset of the current appears at much lower potentials than for the Pt/C electrocatalysts, showing that the removal of the surface-bound intermediate is favoured by the presence of Ru, as in the case of CO stripping (Fig. 3). The presence of shoulders at several potentials during the methanol-stripping scan suggests that the electrocatalysts contains either more than one type of reaction site or crystallites with different activities. Another interesting observation is the presence of broad peaks in the H-upd region for all materials, showing that the electrocatalysts were not completely poisoned by methanol adsorption.

The methanol-stripping peaks for Pt/C catalysts can give support for the results in Fig. 7. Pt/SWNT presents higher currents for methanol electrooxidation (Fig. 7) and also a stripping peak starting at lower potentials (Fig. 8). But Pt/MWNT presents a larger stripping charge indicative of a higher active surface area than Pt/Vulcan XC-72 (Fig. 8) which explains the larger currents for Pt/MWNT than for Pt/Vulcan XC-72 (Fig. 7).

Fig. 9 shows the results for a single DMFC where the anode of the MEA was supplied with $2\,mol\,L^{-1}$ methanol solution and the counterelectrode with oxygen humidified and pressurised to 0.3 MPa at the same temperature of the

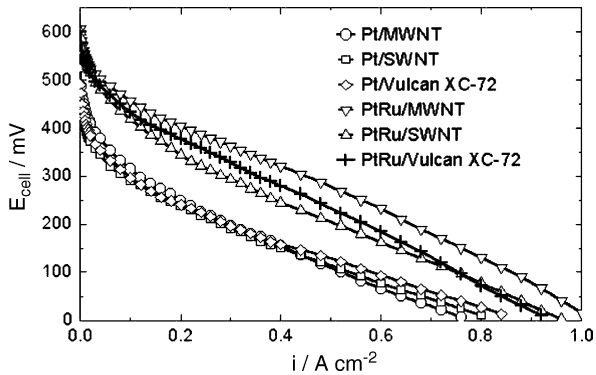

Fig. 9. Potential vs. current density curves for Pt/C and PtRu/C anodes with $0.4\,mg$ noble metal cm^{-2}. Cathodes with 20 wt.% Pt/C (E-TEK, $0.4\,mg\,Pt\,cm^{-2}$). Nafion® 115 membrane. Anodes fed with $2\,mol\,L^{-1}$ methanol solution at room temperature and atmospheric pressure. Cathodes fed with O_2 humidified at 90 °C and 0.3 MPa. Current density with respect to geometric area.

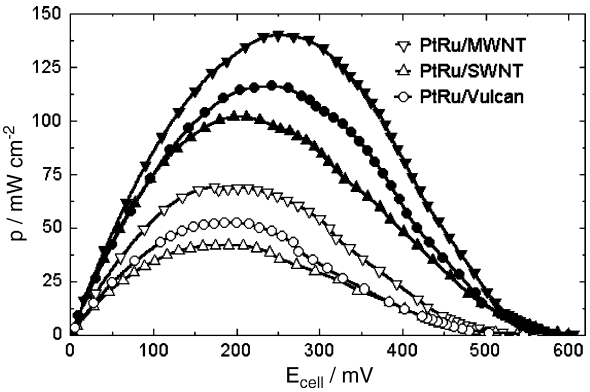

Fig. 10. Power density vs. cell potential for PtRu/C anodes. Open symbols: 70 °C, pO_2 = 0.1 MPa; solid symbols: 90 °C, pO_2 = 0.3 MPa. Other conditions as in Fig. 9.

cell (90 °C). As expected, anodes with PtRu/C present better performances than those with Pt/C. The fact that the results for the Pt/C materials with different supports are similar indicates that the metal contaminants in the nanotubes do not contribute to the performance, at least under practical operational conditions. Among the PtRu/C anodes, the best performance was achieved with the PtRu/MWNT catalyst, while that of the PtRu/Vulcan XC-72 is somewhat above that of the PtRu/SWNT. These results in the DMFC contrast with those of the CO tolerance in the PEMFC (Fig. 5) where the performance for the three PtRu/C materials was similar.

Fig. 10 presents the power-density–potential curves obtained in the DMFC with PtRu/C anodes under two different conditions: 70 °C and atmospheric pressure and 90 °C and 0.3 MPa, showing the same clear trend as the cell potential versus current density data in Fig. 9. The MEA containing the PtRu/MWNT electrocatalyst produced a higher power density compared with PtRu/Vulcan XC-72 and PtRu/SWNT. The maximum power densities show that reasonably good single-cell performances, with power densities exceeding 100 mW cm^{-2} were attained in a DMFC with MEAs containing only 0.4 mg PtRu cm^{-2}, in particular with PtRu supported on MWNT. This shows that careful choice of the anode structure is important to maximise the MEA performance in the DMFC and that the load of PtRu electrocatalyst can be reduced significantly from the 2–10 mg Pt cm^{-2} levels that are usually employed in these fuel cells [11].

4. Conclusions

The results of this work show that the alternative preparation method of the Pt/C and PtRu/C catalysts by impregnation of the carbon support material with the precursors in ethanol followed by drying and reduction in a hydrogen atmosphere produces very active materials for the H_2/CO and methanol oxidation reactions. The carbon nanotubes contain Ni, Fe and other contaminants whose presence seems to help in lowering the potentials for the onset of CO oxidation. A high performance was achieved for the oxidation of H_2 + 100 ppm CO with PtRu deposited on nanotube supports, with an overpotential of about 100 mV at 1 A cm^{-2}, although this is similar to that obtained with PtRu supported on Vulcan XC-72. Results for the DMFC showed power densities exceeding 100 mW cm^{-2} at 90 °C and 0.3 MPa, particularly for PtRu/MWNT. The overall results show that multiwall carbon nanotubes produce PtRu/MWNT catalysts with better performance than on other supports, particularly with respect to those prepared with the traditional Vulcan XC-72 carbon powder. It is expected that progress in the technology of producing nanotubes will make the cost of these alternative support materials to come down to acceptable levels.

Acknowledgments

The authors thank the financial support of the Fundação de Amparo a Pesquisa do Estado de São Paulo (FAPESP 01/12169-2 and 99/06430-8), Conselho Nacional de Desenvolvimento Científico e Tecnológico (CNPq) and FINEP, Brazil. The authors also thank Vania Cardoso Fernandes and Carlos Bento for the XRD and EDX experiments, respectively.

References

[1] A.M. Castro Luna, G.A. Camara, V.A. Paganin, E.A. Ticianelli, E.R. Gonzalez, Eletrochem. Commun. 2 (2000) 222–225.
[2] G.A. Camara, M.J. Giz, V.A. Paganin, E.A. Ticianelli, J. Electroanal. Chem. 537 (2002) 21–29.
[3] T.J. Schmidt, M. Noeske, H.A. Gasteiger, R.J. Behm, P. Britz, W. Brijoux, H. Bönnemann, Langmuir 13 (1997) 2591–2595.
[4] W.F. Lin, T. Iwasita, W. Vielstich, J. Phys. Chem. Sect. B 103 (1999) 3250–3257.
[5] A. Pozio, L. Giorgi, E. Antolini, E. Passalacqua, Electrochim. Acta 46 (2000) 555–561.
[6] S.J. Lee, S. Mukerjee, E.A. Ticianelli, J. McBreen, Electrochim. Acta 44 (1999) 3283–3293.
[7] T. Iwasita, F.C. Nart, J. Electroanal. Chem. 317 (1991) 291–298.
[8] P.A. Christensen, A. Hamnett, J. Munk, G.L. Troughton, J. Electroanal. Chem. 370 (1994) 251–258.
[9] A. Kabbabi, R. Faure, R. Durand, B. Beden, F. Hahn, J.-M. Leger, C. Lamy, J. Electroanal. Chem. 444 (1998) 41–53.
[10] H.A. Gasteiger, N.M. Markovic, P.N. Ross Jr., J. Phys. Chem. 99 (1995) 8290–8301.
[11] M.P. Hogarth, T.R. Ralph, Platinum Met. Rev. 46 (2002) 146–164.
[12] T. Bein, G.D. Stucky, Chem. Mater. 8 (1996) 1569–1570.
[13] N.M. Rodrigues, A. Chambers, R.T.K. Baker, Langmuir 11 (1995) 3862–3866.
[14] G.E. Gadd, M. Blackford, S. Moricca, N. Weebb, P.J. Evans, A.M. Smith, G. Jacobson, S. Leung, A. Day, Q. Hua, Science 277 (1997) 933–936.
[15] T. Kyotani, L. Tsai, A. Tomita, Chem. Commun. (1997) 701–702.
[16] J.G.V. Romero, C.A. Luengo, J.G. Huber, J.M. Rosolen, Química Nova 25 (2002) 59–61.
[17] L.A. Montoro, C.A. Luengo, J.M. Rosolen, E. Cazzanelli, G. Mariotto, Diamond Rel. Mater. 12 (2003) 846–850.

[18] A.L.N. Pinheiro, A. Oliveira-Neto, E.C. de-Souza, J. Perez, V.A. Paganin, E.A. Ticianelli, E.R. Gonzalez, J. New Mater. Electrochem. Syst. 6 (2003) 1–8.
[19] A.R. West, Solid State Chemistry and its Applications, Wiley, Chichester, 1984, p. 734.
[20] V.A. Paganin, E.A. Ticianelli, E.R. Gonzalez, J. Appl. Electrochem. 26 (1996) 297–304.
[21] W.H. Lizcano-Valbuena, V.A. Paganin, E.R. Gonzalez, Electrochim. Acta 47 (2002) 3715–3722.
[22] X.P. Gao, F.X. Wang, Y. Liu, G.L. Pan, S. Li, J.Q. Qu, F. Wu, H.T. Yuan, D.Y. Song, J. Electrochem. Soc. 149 (2002) A1616–A1619.
[23] M. Watanabe, in: W. Vielstich, H. Gasteiger, A. Lamm (Eds.), Handbook of Fuel Cells – Fundamentals, Technology and Applications, vol. 2, Wiley, 2003, pp. 408–415 (Chapter 31).
[24] J.-B. He, C.-L. Chen, J.-H. Liu, Sens. Actuators B 99 (2004) 1–5.
[25] C. Roth, N. Martz, H. Fuess, J. Appl. Electrochem. 34 (2004) 345–348.